

# Magnetic Dipole Levitation - Simulation and Control Optimisation

Samuel Schimanski

**Abstract**—This project aimed to produce a model of dipole-dipole interactions for use in the development of two-coil vertical levitation systems. Furthermore, several controller topologies were to be evaluated for the determination of the most efficient method of control in a vertical levitation system. The research involved the development of dipole-dipole interactions in the Simulink environment along with the required PID, LQR, and LQG controllers. Under realistic conditions i.e., additive disturbance, the controllers were evaluated in terms of their excess power consumption. A physical vertical levitation system was then produced to validate the dipole-dipole model and assess the energy efficiency of the simulated controller topologies.

Construction of the levitation artifact, OS-1, saw the validation of the dipole-dipole model. There was good agreement between the PID controller values which would theoretically stabilize the system and the values in which the physical system was stabilized. Furthermore, the evaluation of the PID controller in terms of its power consumption saw the average consumption differ by only four watts from the simulated results. With good agreement between the simulated and physical power consumption of the PID controller, conclusions were drawn from the simulated results of the PID, LQR, and LQG controllers. The LQR and LQG controllers showed improvements of 4.21% and 4.22% when compared with the PID controller respectively. From this, it can be seen that the LQG controller would offer optimal energy efficiency given a sufficiently accurate system model.

This research provides valuable insight into the optimization of control methods for minimizing power consumption within a two-coil vertical levitation system. Additionally, this research provides and validates a generalized model of dipole-dipole interactions which is applicable to generic coaxially constrained two-coil systems. The limitations of this research included the use of a coaxially constrained model and the lack of physical implementations of the optimal controllers simulated. Future works should include further physical implementation of the discussed controller topologies and the implementation of a model that is not constrained coaxially for comparison.

**Index Terms**—Dipole levitation, simulation, classical control, optimal control, two-coil system, PID, LQR, LQG, efficient control

## LIST OF VARIABLES

$\alpha$	Vertical magnetic force growth rate, $\text{Ns}^{-1}$
$\beta$	Sensor gain, unit-less
$\gamma$	Current source gain, unit-less
$\Phi_F$	Magnetic flux floating coil, Wb
$\Phi_L$	Magnetic flux levitator coil, Wb
$B_r$	Radial magnetic field, T
$B_{z0}$	Axial field at initial position, T

$B_z$	Axial magnetic field, T
$D$	Derivative gain, unit-less
$f$	Frequency, Hz
$F_z$	Force in the z direction, N
$G$	Transfer function, unit-less
$g$	Gravity, $\text{ms}^{-1}$
$I$	Current, A
$I_F$	Floating coil current, A
$I_{L0}$	Initial levitator current, A
$I_L$	Levitator current, A
$J$	Quadratic cost function, unit-less
$L_F$	Self inductance floating coil, H
$L_L$	Self inductance levitator coil, H
$m$	Mass, kg
$M_{LF}$	Mutual inductance between levitator and floating coil, H
$N$	Cross term matrix, unit-less
$N_F$	Floating coil turns, unit-less
$P$	Proportional gain, unit-less
$Q$	State variable weight, unit-less
$R$	Control input weight, unit-less
$r$	Radius, m
$R_L$	Levitator coil radius, m
$s$	Laplacian s, complex variable
$U$	Potential energy, J
$z$	Vertical height, m

## I. INTRODUCTION

Nuclear fusion has long been seen as the holy grail of clean energy [1]. Fueled by hydrogen isotopes deuterium and tritium, fusion offers the potential for near-limitless energy production due to hydrogen isotopes natural abundance [2] [3].

Many different approaches have been and are being taken to achieve fusion. Arguably the world-leading approach being magnetic confinement [4]. The most notable reactors are Tokamaks and Stellarators although, other forms of magnetic confinement reactors exist such as the levitated dipole reactor [5]. First theorized by Akira Hasegawa and later brought to life by a team at Massachusetts Institute of Technology (MIT) in the early 2000s under the name, “Levitated Dipole Experiment” (LDX) [6]. As the name implies, the device involves a magnetic dipole which is levitated by an external force in order to be used for plasma confinement. Specifically, an overhead magnet is used for levitation. This formation is inherently vertically unstable, requiring a feedback loop and control system to maintain stability. This paper discusses the development of a model of dipole-dipole interactions and

the design and evaluation of several controllers which ensure vertical stability. As a fusion reactor is a power system at heart, efficiency is a fundamental aspect to be considered. Any unnecessary power consumption during the system's runtime will harm the reactor's bottom line in terms of net power production. This includes excess levitator excitation.

Thus, with efficiency in mind, these controllers will be evaluated to determine any inherent advantages or disadvantages in terms of efficient power use. Furthermore, the accuracy of the produced models are to be assessed to determine their reliability in being applied to arbitrary coil geometries.

## II. BACKGROUND RESEARCH

During preliminary research, the author was unable to find any publication with strong similarities to the project at hand. Although, several research papers were found that cover the design and build of attractive levitation devices including the modeling of said systems at a simplified level i.e., filamentary coils [7] [8]. The following background research will include electromagnetic stability, classical control, optimal control, and any existing solutions albeit adjacent ones.

### A. Vertical Stability

Earnshaw's theorem pertains to the stable stationary equilibrium of a collection of point charges. It states that solely by using the forces from electrostatic interactions of these point charges, a stable static equilibrium cannot be achieved [9]. The same applies to electromagnetic stability. Stability in this sense would require that if the system would be exposed to small perturbations i.e., a nudge, the system would fall back into its equilibrium position regardless of the direction of said perturbation.

Mathematically this means that all the field lines would point inwards toward the equilibrium position but as Gauss's law states "divergence of any possible electric force field is zero in free space", The stability of a magnetic source can not be assured passively [10]. This leads to the need for a feedback controller.

$$\nabla \cdot \mathbf{F} = \nabla \cdot (-\nabla U) = -\nabla^2 U = 0 \quad (1)$$

### B. Methods of Control

A variety of control methods for attractive levitation exist, the two primary ones are optical-based and magnetism-based. Optical-based levitation consists of optical sensors to determine the position of the floating magnet. Some such notable uses are the RT-1 and LDX systems [7] [11].

Magnetic field-based control would employ the use of devices such as a Hall effect sensor. The measured field strength is converted to a voltage via the Hall effect and is then used in a control loop [12]. Both methods provide adequate positional measurements although, optical sensors have a greater immunity to stray magnetic interference from the coils. With either of these 'positional' measurements, the current through the levitator coil can be adjusted to provide the appropriate force on the floating coil to sustain levitation.

How heavily the levitator coil's current is changed depends on the difference between the set point and the measured position, along with the gain values of the controller. Many types of controllers exist, typically falling under two main branches, classical control and optimal control.

1) *Classical Control*: Classical control theory deals with linear time-invariant, single input single output systems (SISO) with emphasis on frequency domain analysis making use of such tools as Bode, root locus, and Nyquist plots [13]. The most common controller used in classical control is the proportional-integral-derivative (PID) controller due to its ease of implementation and fast tuning, alternatively, there also exists the 'bang-bang' controller which implements a purely on-off state depending on the error signal [14] [15].

A PID controller consists of three components, proportional, integral, and derivative [14]. Each component acts individually on the error signal, in the independent form, before being summed together to form the new input to the plant, the plant being a representation of the system dynamics [14]. By appropriately tuning each component one can obtain an output response that produces a favourable response from the plant.

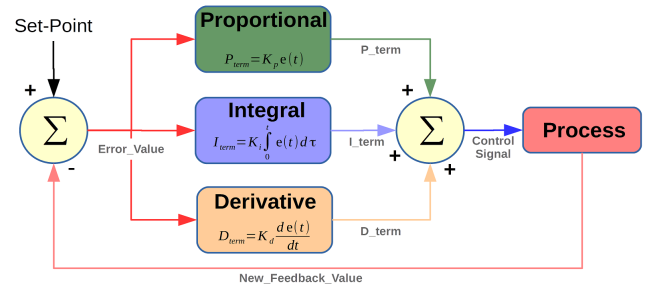


Fig. 1. PID controller block diagram

2) *Optimal Control*: Optimal control unlike classic control, takes a more mathematical approach. Optimal control deals with systems in the time domain, using mathematical optimization to control the dynamics of a system over a given time period in such a way that some objective function is optimized [16]. One notable optimal control system is the Linear Quadratic Regulator (LQR). The LQR optimizes a cost function based on two input parameters, Q and R, either optimizing for performance or energy saving respectively eq. 2.

$$J = \int_0^{\infty} (x^T Q x + u^T R u + 2x^T N u) dt \quad (2)$$

### C. Existing Solutions/Literature Reviews

As previously discussed there have been several publications on and surrounding the control schemes for attractively levitated systems. The most notable of these publications is that of RT-1, LDX, and the APEX-D [7] [8] [17]. All of these systems implement a form of attractive levitation with optical measurement feedback. Although these projects operate at vastly different scales to the proposed system, they all implement the same fundamentals thus, demonstrating the solvable nature of the system.

1) *RT-1*: The RT-1 or Ring Trap experiment modeled a large-scale two-coil system with the use of a force equilibrium equation as its coil motion characteristics. Modeling equilibrium conditions to produce cancellation of the gravitational forces via the forces of interaction between the floating coil and levitator coil [7].

$$m \frac{d^2 t}{dt^2} = 2\pi R_L N_F I_F B_r - mg \quad (3)$$

Although, a coil in free space generally has six degrees of freedom (DOF), positions (x, y, z), tilts ( $\theta_x, \theta_y$ ) and rotation  $\theta_z$  the RT-1 team consider the coils to be coaxially constrained when developing their coil motion equations [fig. 2] [7].

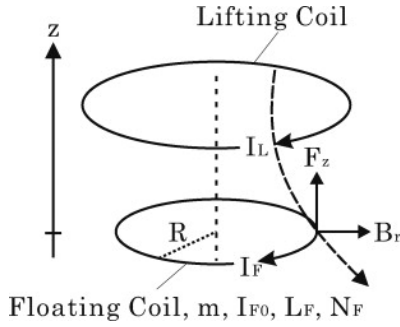


Fig. 2. Co-axially constrained coils

RT-1 was able to produce a large-scale levitation scheme with the use of the previous force equilibrium equation 3. This method of system modeling provides a relatively simplistic method of representing coil motion although, it offers no knowledge of the coil's other five degrees of freedom. Therefore, the system becomes more of a guessing game in terms of designing for the stability of the other degrees of freedom that are affected by coil geometry. Within RT-1's experiments, they required correction coils to correct the floating coils misalignments of tilt and slide likely caused by their limited knowledge of the coil's remaining five degrees of freedom [18].

2) *APEX-D*: The APEX-D experiment improves upon RT-1's original works by implementing stability criteria for tilt and slide of the F-coil [17].

The APEX-D project makes use of the same force equilibrium criteria as RT-1 but slightly improves on their design methods by implementing a tilt and slide criteria [17]. The APEX-D team considered perturbations from the equilibrium position of the coil and the Lorentz force on the coil while contained within the magnetic field of the levitator coil. The Lorentz force is an electromagnetic force describing the force on a moving electric charge by an external magnetic field [19]. For slide and tilt, the following stability criteria were produced 4 5.

$$0 < \frac{\partial B_z}{\partial r} \Big|_{z=0} \quad (4)$$

$$0 < B_{z0} + r_F \frac{\partial B_r}{\partial z} \Big|_{z=0} \quad (5)$$

Using these tilt and slide stability criteria, the APEX-D team gained an advantage over systems like RT-1 as they could accurately determine the system geometry required for passively stable tilt and slide modes. However, one disadvantage of this approach is that they only knew the ranges of stability but had little knowledge of how the system would behave in this range. That is, they did not know how stable the system was in a given region e.g., marginally or very stable, and were unable to determine what force would be required to end the system's stability or what natural oscillations may be seen.

3) *LDX*: The LDX team can be considered a leader in terms of their control system for an attraction-based magnetic levitation system. The reason for this is in their system modeling. Where the likes of RT-1 and APEX-D considered their floating coil coaxially constrained, the LDX team allows their model to make use of all six degrees of freedom (6-DOF) [8]. Although computationally a much greater task, the use of such a model allows for greater certainty of stability for arbitrary coil geometry eq. 12.

$$F_{\text{magnetic}} = \nabla \mathbf{M}_{LF} \frac{(\mathbf{M}_{LF} \Phi_F - L_F \Phi_L)(\mathbf{M}_{LF} \Phi_L - L_L \Phi_F)}{(L_L L_F - M_{LF}^2)^2} \quad (6)$$

With this equation, the LDX team was able to model the motion of their floating coil with an appropriate controller topology to sustain levitation. The controller in question was a digitally implemented PID controller [8]. One disadvantage seen in the LDX team's control design lies in their choice of classical control despite having a well-defined single input multiple output system (SIMO). With the use of optimal control, the LDX team would have been able to ensure a controlled system with far greater optimizations than could be made by 'hand' with classical control methods.

Another advantage the LDX team held was their use of filtering. While the other mentioned teams only used standard low-pass filtering, LDX implemented a Kalman filter [20]. A Kalman filter, also known as a Linear Quadratic Estimator (LQE), is a recursive digital filter that uses a series of measurements over time, statistical noise, and the state space representation of a system to provide more accurate state estimations of the system than can be measured in some cases. [fig. 3] [21].

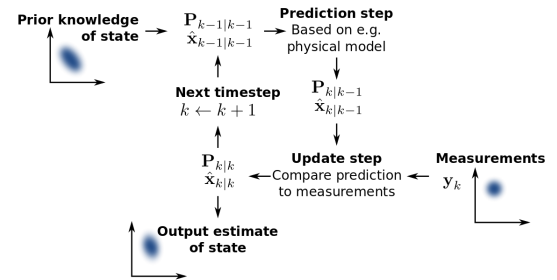


Fig. 3. Kalman filter state diagram

With this, LDX was able to further reduce the effects of measurement and process noise within their system, thereby making their system more robust and efficient as less unnecc-

essary excitation of the levitator coil would ensue. This is due to less noise propagating into the control signals.

### III. DESIGN AND IMPLEMENTATION

The design of OpenStar-1 (OS-1) was broken down into it's two major components, the simulation design and the physical build design. The simulation design aimed to accurately capture the most important aspects of the system in a generalized form. This allowed for the simulation to be easily applicable to arbitrary two-coil systems. While the physical build aimed to validate the results seen in the simulations.

#### A. Simulation Design

The aspects of the system deemed crucial to building an accurate model are as follows.

- The coil dynamics
- The current source response
- The sensor feedback
- The controller

These aspects were considered crucial due to their large impact on the system dynamics as coil dynamics define the coil-coil interactions, and the current source and sensor feedback hold the largest time delays and gains seen in the system. Additionally, the controller was required to be modeled as it provided the necessary alterations to the error signal to produce stable levitation.

1) *Modelling Coil Dynamics:* In order to model the coil dynamics in an easy-to-understand, generalized form, RT-1's co-axially constrained coil equation of motion was used [3].

This method was chosen over the arguably more sophisticated 6-DOF approach taken by LDX, due in part to computational ease, as this method only requires readily available system data such as amp-turns, coil dimensions, etc. Additionally, although the 6-DOF model offered information about the states of the floating coil in all directions, this level of detail was not necessary for designing a vertically stable two-coil system with arbitrary coils as the less labour-intensive tilt and slide stability curves offered by APEX-D were available [17].

Coil motion was linearized as per [17] by equating the L-coil current to,

$$I_L = I_{L0}(1 + I/I_{L0}) \quad (7)$$

From this, coil motion can be characterized via the following transfer function.

$$G_{\text{coil motion}} = \frac{1}{I_{L0}\alpha} \frac{1}{s^2/(g\alpha) - 1} \quad (8)$$

With this generalized transfer function making the base of the coil-to-coil interactions, all remaining simulation aspects are derived purely from the surrounding system. That is, all other system aspects are at liberty to be chosen by the responsible engineer.

2) *PD Controller:* As maglev systems typically have proportionally small integral gains [17], a PD (proportional-derivative) controller was simulated as the first controller topology. In additive form, this takes the expression,

$$G_{PD} = P(1 + \frac{D}{P}s) \quad (9)$$

A variation of the PID controller was chosen as the first controller topology due to its wide use in industry and for its well-understood characteristics [14]. Additionally, the intuitive tuning controls allow for just about anyone to obtain a satisfactory system response given some trial and error.

Much like the remaining controller topologies this control system is to be implemented first in a Simulink environment to ensure system stability and then again digitally in a real-time operating environment.

3) *LQR Controller:* The LQR was a chosen controller topology for this project due to its ability to produce an optimal gain matrix from a set of weighting coefficients, Q, R, and the state space representation of a system. These weights represent the importance of similarity to the system set point and the importance of a small control effort respectively [22].

Much like as seen in classical control with the PID controller, without the integral action, the steady-state value of the system will not be equivalent to the set point provided, assuming a step input [13]. The steady-state value of a system is the final output produced by the plant once all system dynamics have died down. This problem can be solved in two ways in optimal control, a pre-filter or integral control. Integral control, much like in a PID controller, looks at the error between the set point and the system's output state variable and integrates this error over time to bring the control signal to a point where the set point is reached. The pre-filter on the other hand is essentially a gain block determined by the known state space model. This gain pushes the initial control signal to where it should be in order to produce the desired outcome [22].

The pre-filter has the benefit that it acts instantaneously on the system although, the pre-filter may also produce a steady-state error with differences between the modeled state space system and the actual system characteristics. Integral control offers zero steady-state error but requires time to ramp up, time in systems such as controlled levitation that is not likely available. Therefore, a combination of the two has been used in the project for both optimal controllers, LQR and LQG [4]. This was done to take full advantage of both zero steady-state error and the initial boost in the control signal to push the system within the ballpark of its required value. This prevents the system from having time to fall away from its linearized equilibrium before an appropriate control signal has been achieved. Just the use of integral controller may not apply feedback fast enough to prevent the system from falling out of vertical stability.



design difficulties. This linearization enabled a relatively easy design of the control system but this also imposed a limitation on the system. This is, as the system moves further away from its linear region the system dynamics can differ vastly and therefore render the control system useless.

### B. Physical Build Design

The system's physical design can be broken down into six main segments. The design of the "coils", enclosure, and evaluation components along with the selection of the sensors, additional control components, and real-time operating system.

1) *Coil design*: As discussed prior, the system revolves around two coils, the levitator and the floating "coil". The floating coil in this case is a permanent magnet for simplicity. When selecting the permanent magnet two main criteria were required. The magnet must have a high field strength-to-weight ratio and the magnet must be short, wide, and cylindrical to better approximate a circular current loop. With these requirements in mind, an N45 neodymium magnet of diameter 30mm, height 10mm, and weight 53g was chosen.

2) *Levitation Coil*: The levitator coil design is split into two main design areas, the coil design and the bobbin design.

The design of the levitator coil had to take into account several factors including the distance from the floating coil, its field strength, and dimensions. In order to ensure slide and tilt stability, plots of stable regions had to be developed with the floating coil's dimensions in mind 7 6.

Slide and tilt stability plots were produced for the dimensions and approximated amp-turns of the floating coil 4 5

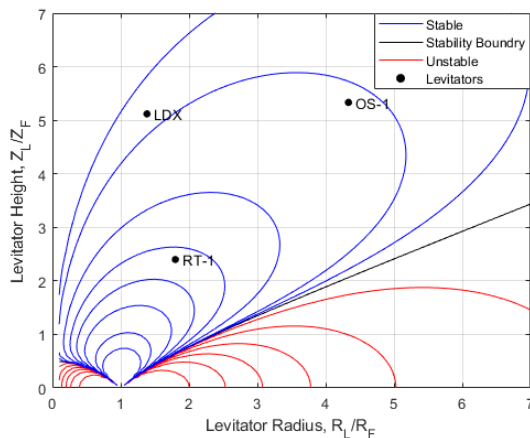


Fig. 6. Slide stability contour with levitator radius normalized by floating coil radius

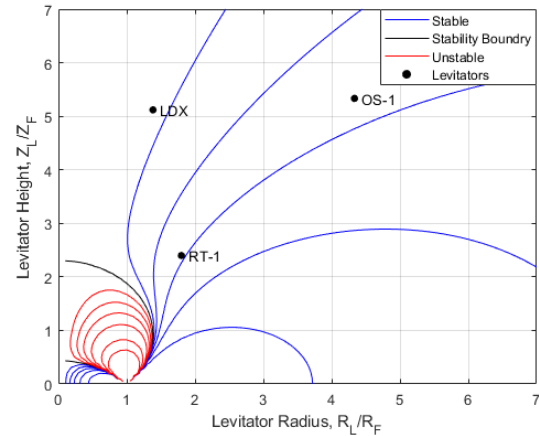


Fig. 7. Tilt stability contour with levitator radius normalized by floating coil radius

From 6 7, the acceptable levitator coil dimensions could be seen.

In order to optimize the coil design the levitator's radius was chosen such that the field strength at the edge of the floating magnet would be maximized while still maintaining slide and tilt stability.

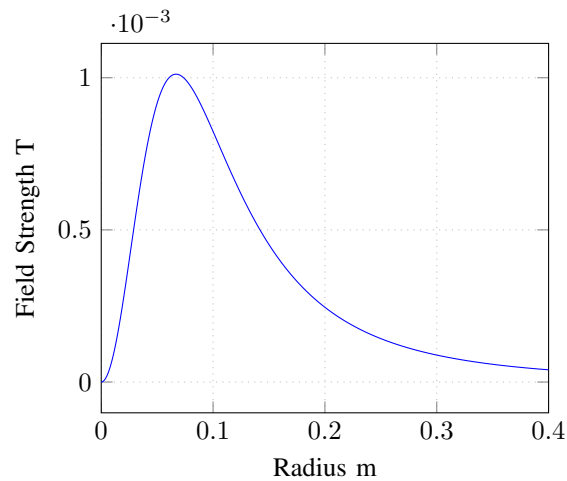


Fig. 8. Field strength at floating coil radius with changing levitator radius

With an optimized geometry, the number of turns in the levitator was chosen such that nominally 7A would be required to keep the floating coil at equilibrium. In this case, 350 turns were required. These parameters allow for substantial vertical oscillations before the supplied current source would no longer be able to bring the coil back to its equilibrium position, as the supplied current source is limited to 10A.

3) *Levitation Bobbin*: Due to the relatively high power dissipation expected within the levitator coil, extra precautions had to be taken to reduce the likelihood of premature thermal failure. A thermal Finite Element Analysis (FEA) study was performed to determine how much heat could be dissipated at nominal load (110 W) with differing bobbin materials and geometries. Results showed that an aluminum bobbin with

heat-sinking fins lining the bobbin's top face would suffice in keeping the steady-state temperature below 50 °C. While the addition of a fan would see the steady-state temperature decrease to 36 °C at its peak 9.

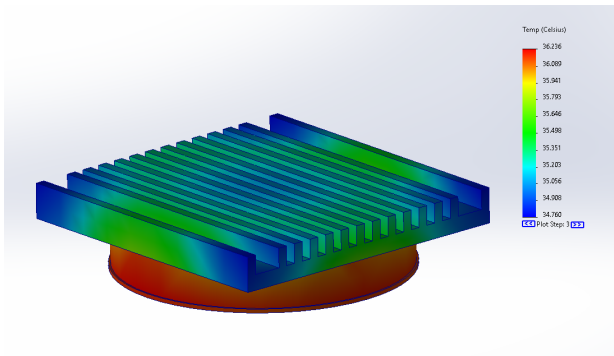


Fig. 9. 110 W thermal load test results, simulated

Alternate designs were also trialed 10, although as there were very little size constraints on the bobbin a larger surface area bobbin was selected to further improve thermal characteristics.

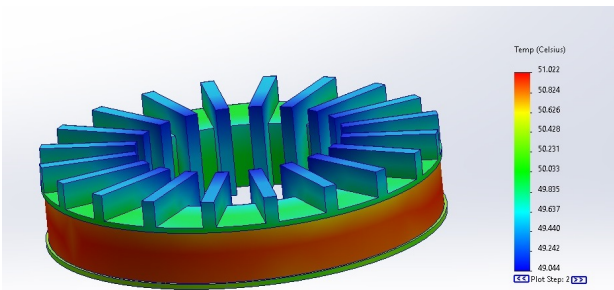


Fig. 10. 110 W thermal load test results, alternative bobbin design, simulated

Aluminium was chosen for the bobbin material not only for its thermal characteristics but also for its relative abundance and more importantly its non-ferrous properties [24]. Being non-ferrous allowed for the inner section of the bobbin to be completely filled while still maintaining an “air core”. Filling the inner section of the bobbin gave the levitator coil greater thermal mass and therefore made it more resistant to temperature changes. Additionally, more space was available for heat-sinking fins further improving the thermal characteristics of the levitator coil/bobbin.

4) *Enclosure Design:* The enclosure surrounding the levitator was designed with modularity in mind. That being, the enclosure was designed in such a way that further additions to the system such as mounts, sensors, etc could be added with ease. Furthermore, the enclosure was also designed such that maintenance would not pose much difficulty.

This resulted in an enclosure constructed from 40x40mm extruded aluminum with dual rail t-slots. This specific material offers competitive strength-to-weight ratios when compared

with steel [25], while the specific shape allows for the mounting of a variety of hardware.

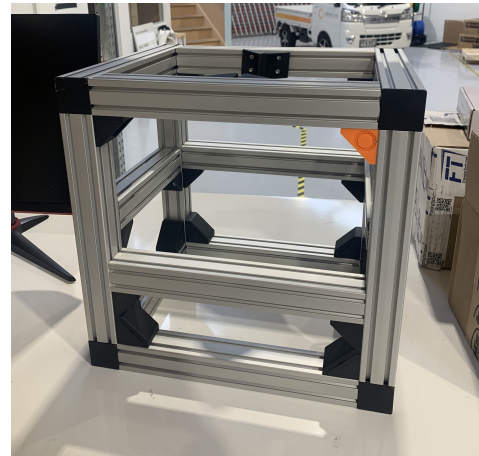


Fig. 11. System enclosure, prior to hardware mounting

Alternatives considered included a 3-D printed enclosure as all parts produced could be purpose-built to ensure minimal material waste. Due to the significantly lower strength of Polylactic Acid (PLA), this alternative was discarded [26].

5) *Real Time Operating System:* A real-time operating system was a hard constraint within this project due to the fast dynamics of the plant. These fast dynamics require real-time levels of response in order to ensure the system remains vertically stable.

Beckhoff's TwinCAT 3 was chosen as the operating system for this project. TwinCAT is a widely used control and automation platform and was chosen as this project's real-time operating system for several reasons. Reasons include its Simulink-TwinCAT interface, its plug-and-play control modules, and the large variety of control toolboxes [27].

6) *Sensor Selection:* Sensor selection was a heavily constrained area of the project. The chosen sensors had to adhere to the following criteria.

- Must be amplitude modulated
- Must cover distances of 5.2m
- Must have a time response of less than 10ms
- Must have resolution of less than 1mm

With these conditions in mind, the LV-NH300 sensors were chosen [28]. In addition to meeting all the above conditions, the sensors offered several other features. Including, multi-sensor integration via a coupled amplifier design and PLC integration via the EtherCAT communication bus [28].

The LV-NH300 sensors come in transmitter-receiver pairs and therefore 16 total sensors are fitted around the enclosure to capture the floating coil's five degrees of freedom. Finally, purpose-built brackets provided with the sensors allow for fine positional tuning of the sensors in all directions ensuring ease of use [28].

Several other sensor options were considered, such as the SICK retroreflective sensor and the Di-Soric LAT45-10MIU-B5. [29] [30]. Both of these sensors offered the range and

time response required but lacked in resolution, offering at best 1mm resolution. Additionally, it was unclear whether or not these sensors were amplitude-modulated.

7) *Control and Data Acquisition Components:* Additional control components were required as an interface between the real-time operating system and the plant. For integration with the pre-selected real-time operating system, Beckhoff modules were selected.

Specifically, an analog measurement unit (EL3104) and an analog output unit (EL4034) were selected for this project to collect power data and control the supplied current source respectively [31] [32]. Again, these modules were chosen for their ease of integration with the chosen real-time operating system. Additionally, the modules offered high resolution and response times faster than the required PLC cycle time of 2ms thus, ensuring adequate control and data acquisition speeds. Finally, a bridging PCB was produced to convert the

voltage and current readings across the levitator magnet into voltage signals measurable by the Beckhoff modules. The measurement range of the Beckhoff modules was  $\pm 10V$  and the maximum expected voltage and current seen across the levitator were 30 V and 10 A respectively. With this in mind, a range of components including hall effect sensors, op-amps, and precision resistors were chosen to transform these current and voltage signals into appropriately scaled voltage signals [12].

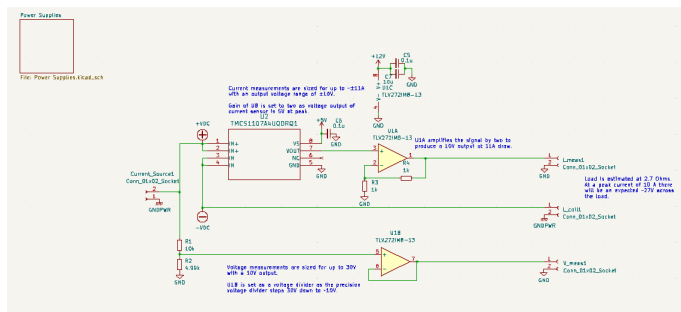


Fig. 12. Kicad schematics, bridging power measurement board

The PCB was designed with short, wide traces connecting to the hall effect sensor pins in order to prevent traces from breaking due to thermal stresses. Additionally, on-board battery supplies were included to prevent the switching power supply from propagating noise into the IC (integrated circuit) power rails. Finally, precision resistors and op-amp (operational amplifier) ICs were used to ensure precise measurements could be obtained. Although this PCB is not essential in the operation of the control system it does find use as a critical evaluation tool.

8) *Physical System Limitations:* Physical system limitations fall into two main categories, magnetic limitations and component limitations. Magnetic limitations are the limitations in producing an “ideal” magnetic field. That is, due to being

hand-wound along with other un-characterized behaviors the magnetic field produced by the levitator coil is not ideal. These field irregularities can cause minor disturbances when the levitator interacts with the floating coil.

Component limitations include time delays, non-linearities, and component saturation. Time delays are accounted for within the produced simulations and non-linearities have been dealt with by operating all components such as the current source around their linear regions. Component saturation was dealt with by ensuring small control signals were produced while still maintaining a vertically stable system. In terms of the PD controller, this was done by ensuring both the proportional and derivative gains were kept simultaneously small. For the LQR and LQG controllers, this was done by heavily penalizing control effort i.e., R was made magnitudes larger than Q. Doing so not only prevents the control system from driving the current source too hard but also minimizes the power draw of the system.

9) *Firmware Development:* The firmware developed for this project was produced in Beckhoff’s TwinCAT 3. TwinCAT 3 is a control and automation platform developed for working with real-time systems via programmable logic controllers (PLC).

The firmware developed for this project manages all sensor data, computational processes, and implements the digital control loop. Much like the design of the system model, the function blocks were designed to be generally applicable to arbitrary two-coil systems. That is, function blocks containing the controllers and positional measurements have been designed such that few variables need to be changed in order to apply the code to another two-coil system.

As discussed previously the PLC cycle time was set to 2ms in order to allow the control system to respond to the dynamics associated with the plant’s oscillation frequency. 2ms was chosen due to the recommendation that the system should have a response time of at least 100x the plant’s natural oscillation frequency,  $\sim 1$  Hz [33].

Real-time operating systems allow priorities to be set on which task is to be executed first during a cycle. Items deemed of high priority were the positional measurements and the updating of the control loop, as these were the only functions required for stable levitation. Low-priority functions included power measurements and slide/tilt data collection.

The program runs in a cyclical manner, continually repeating the set steps unless an end run-time command is provided [13].

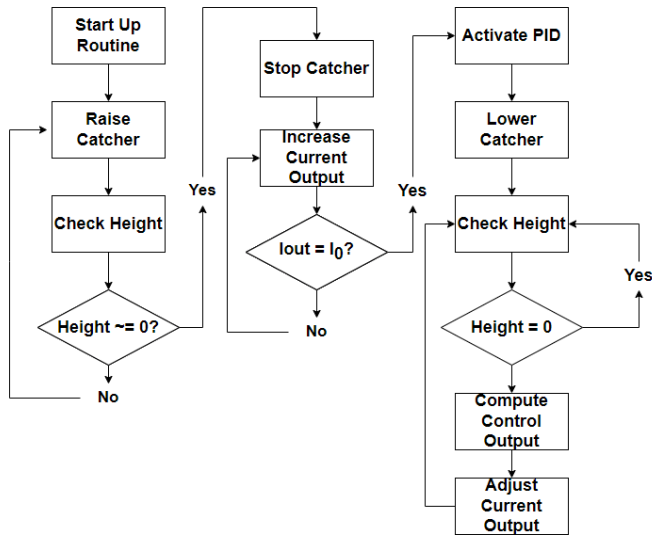


Fig. 13. System process state diagram

IV. EVALUATION

Evaluation of this project is primarily concerned with the accuracy of the simulated model in relation to the physical build. Along with the effective efficiency of the different controller topologies in terms of power consumption of the levitator coil during steady-state operation. Additional evaluation of the system’s thermal characteristics and tilt and slide stability will also be completed.

A. Model Evaluation

After completion of the physical build, several system properties were collected in order to evaluate the system’s likeness to the developed models.

TABLE I  
SYSTEM CHARACTERISTICS

Levitator Coil	
ID	154 mm
OD	158 mm
Height	28 mm
Resistance	2 ohm
# of Turns	350
$I_0$	7 A
Floating Coil	
OD	30 mm
Mass	53 g
Amp-Turns	8250 A.t
Coil-Coil Interaction	
$\alpha$	25

Completion of a Routh-Hurwitz criterion provided a PD stability region defined by a parabolic arch with a minimum proportional gain value of 165 and minimum derivative gain value of 1 14 [34].

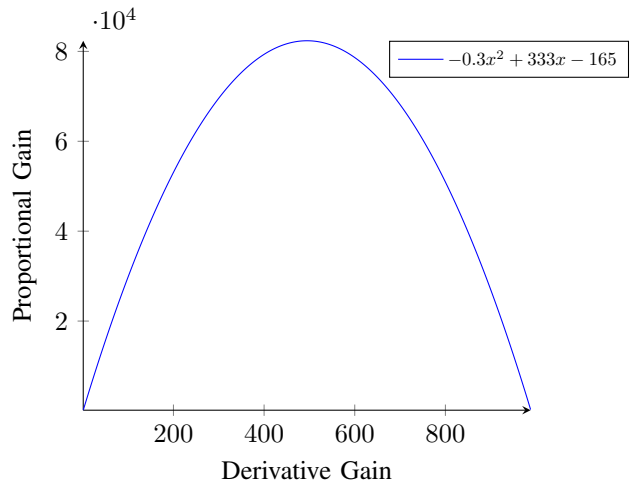


Fig. 14. Stability conditions with varying P and D gains

Due to fast response times, minimal sensor and current source gains the theoretical stability region for this PD controlled levitation device is quite large 14. However, it is practical to contain proportional and derivative gain values to the lower left sector of the graph where both the proportional and derivative gains are small. This is to prevent saturation of control components such as the current source, as the larger set of gains would see the current source attempt to reach values outside of its capabilities and therefore produce an unstable system.

Simulated testing of the system’s proportional gain boundary with a constant derivative gain resulted in a stable system response far above and approaching the boundary when subject to a step input. While below the boundary the system response diverged, as predicted by the system’s Routh-Hurwitz criterion 15.

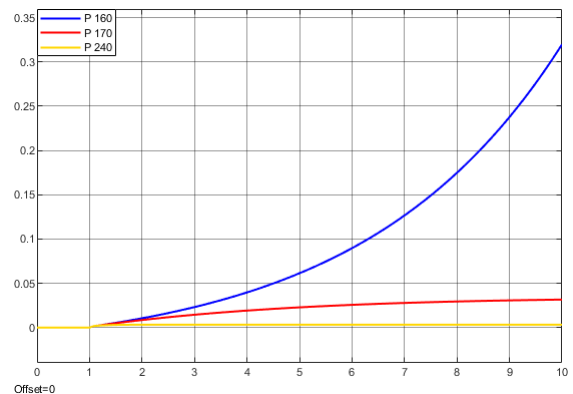


Fig. 15. System response to a step input along the proportional gain lower boundary

Simulated testing was also performed along the boundary of the derivative gain with a constant proportional gain. On and above the derivative gain boundary, the system converged to a steady-state value. When the derivative gain was under the boundary condition the system diverged, much like was

predicted by the Routh-Hurwitz criterion 16.

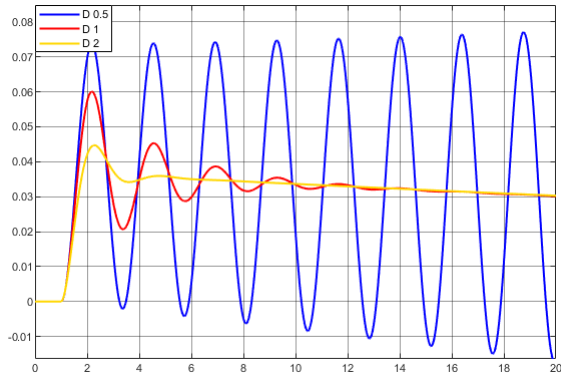


Fig. 16. System response to a step input along the derivative gain lower boundary

Tests were performed on the physical system along lines of constant proportional gain and separately constant derivative gain. Doing so revealed the lower stability boundaries for both proportional and derivative gain within the physical system.

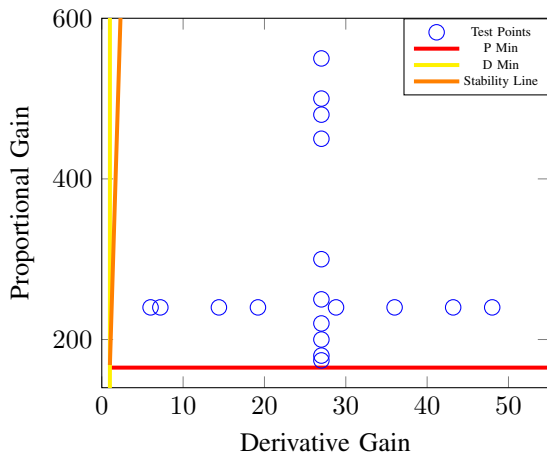


Fig. 17. Stable test flights performed within the calculated stability range

Even with a simplistic system model the PD stability range expected agrees well with the ranges of stability seen during testing. The lower proportional limit seen during testing was 174, only 9 larger than the expected proportional lower limit of 165. The derivative gain lower bound found during testing was 6 while a gain of 1 was expected, therefore, only 5 greater than the expected derivative lower bound. Although not exact, this simple model offers a great starting point for controller development of a two-coil levitation system.

Finally, to ensure the physical system was resilient to perturbations a series of disturbances were placed on the floating coil's vertical position ranging from 1mm-2mm to assess the control loop's ability to maintain its set-point IV-A. Disturbances were performed between 20-40 seconds of flight time.

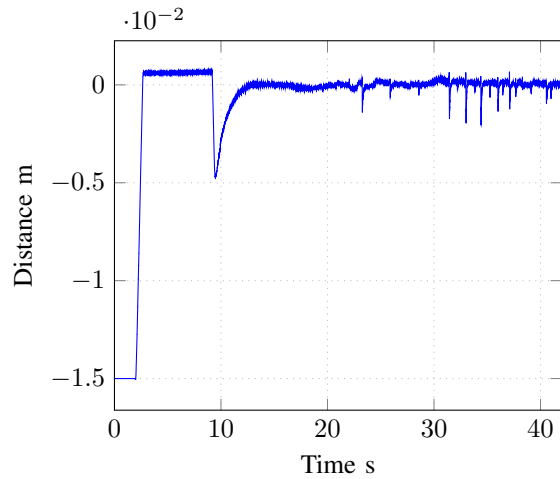


Fig. 18. PID disturbance testing the system's ability to maintain a set height under a series of disturbances

As can be seen, the system was able to stabilize itself after substantial disturbance to its vertical position thus, stabilizability is assured with the PID controller.

Differences between the simulated model and the physical build come from a variety of places. However, the most prominent are likely to be simplified calculations used during the development of the simulated model and inaccurate measurements taken during the physical build characterization. An example of this may be the Amp-turn approximation calculated for the floating magnet.

### B. Slide and Tilt Stability

Slide and tilt stability of the floating coil was designed for by considering the geometries of both coils. Tilt and slide stability plots showed regions where stability would be achieved although, no numerical data on how stable the system was expected to be could be inferred 6 7.

Evaluation of slide stability in both the X and Y directions over a five-minute levitation test showed that the X direction was strictly bound between  $-208\mu\text{m}$  and  $242\mu\text{m}$  while the Y direction was bound between  $-237\mu\text{m}$  and  $219\mu\text{m}$  19. With both directions exhibiting oscillatory motion with an oscillation frequency of 1.3 Hz.

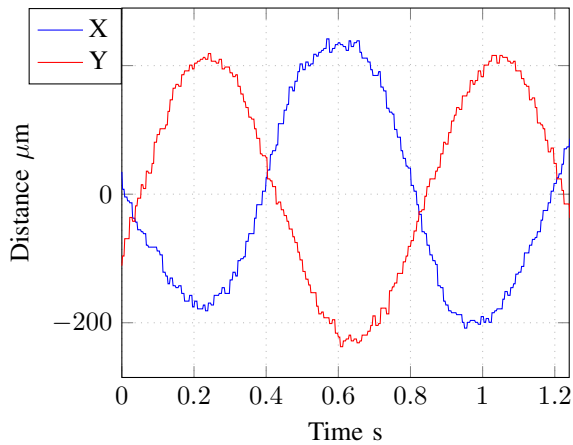


Fig. 19. Slide motion in the X (blue) and Y (red) axes

With only minor deviation from the system's "zero" position despite the oscillatory motion of the floating coil perturbing the system from its equilibrium it is safe to assume slide stability. With the negligible slide in both X and Y directions seen, it can be determined that positioning the levitator coil far from the slide stability boundary likely produces a more slide-stable system.

Similarly, tilt stability was assessed over a five-minute levitation test. The testing showed that there was an angular offset from the zero position along both axes. On average there was a  $1.07^\circ$  offset from the X-axis and a  $0.6^\circ$  offset from the Y-axis. The angle off of the X-axis was bound between  $1.76^\circ$  and  $0.39^\circ$  while the angle off of the Y-axis was bound between  $-0.02^\circ$  and  $1.92^\circ$ .

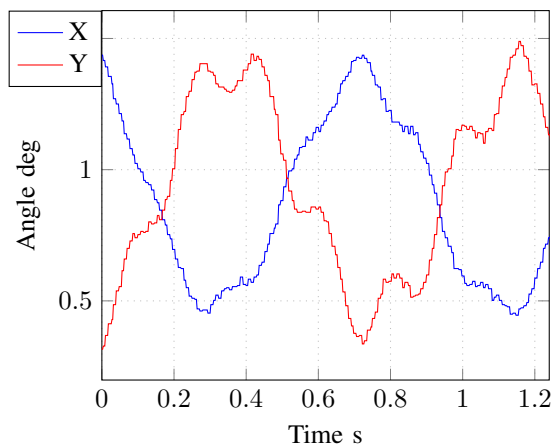


Fig. 20. Tilt motion off of the X (blue) and Y (red) axes

Examining the angular displacement from the X and Y axes it can be seen that the floating coil is tilt stable with a continually oscillating mode, oscillating at a frequency of 1.3 Hz. As the angular displacement is shown to be moving between set bounds passive tilt stability of the system via the magnetic interactions of the levitator coil and floating coil can be confirmed. The angular offset seen in both the X and Y axes can likely be attributed to field irregularities in the two coils. It

should be noted that a similar offset was seen within the RT-1 experiment [18]. This offset was caused by Earth's magnetic field although this is unlikely the case in this scenario due to the scale of the system.

### C. Thermal Evaluation

In order to sustain levitation without premature thermal failure, an appropriate heat-sinking bobbin had to be designed. Thermal testing was performed with a constant 110W power draw and forced convection provided by an overhead fan with a diameter equal to the levitator's outer diameter [35]. Simulated results showed the levitator coil reaching its steady-state temperature after five minutes under a 110W load therefore, the thermal testing was completed over a 10-minute period to ensure steady-state had been reached.

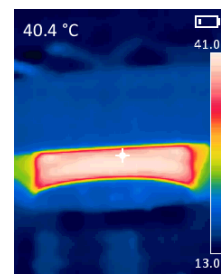


Fig. 21. 110 W thermal load test results

The results of thermal testing showed an error of only 10.7% when compared with the simulated results with the greatest thermal stress being seen around the outer coil face much like in the simulation. This is due to the outer coil face being the only face not in direct contact with a heat-sinking surface. For a simple thermal analysis that assumed the coil to be a solid block of copper, the results of the simulation agree within a tolerable error of the evaluated system.

### D. Controller Evaluation

As previously discussed, several controller topologies were designed for use in this vertical levitation system. The aim was to minimize power draw to ensure limited excess heating in the levitator coil. In order to produce simulations that would accurately represent the system's dynamics two preliminary measurements had to be taken, process noise covariance and measurement noise covariance. Both of these variables have been previously mentioned as the LQG controller makes use of them in producing a noise-tolerant control system [20]. Including these variables within the simulated system offers insight into how each idealized controller would perform under more realistic conditions.

The covariance of measurement noise was determined by ensuring a known set-point was reached and held stationary. From this position sensor data was taken over a two-minute period. By removing the known signal from each data point, only measurement noise was left. From this, the covariance of measurement noise can be calculated as the variance of the remaining noise. The covariance of measurement noise was determined to be  $9.10299e - 12$ .

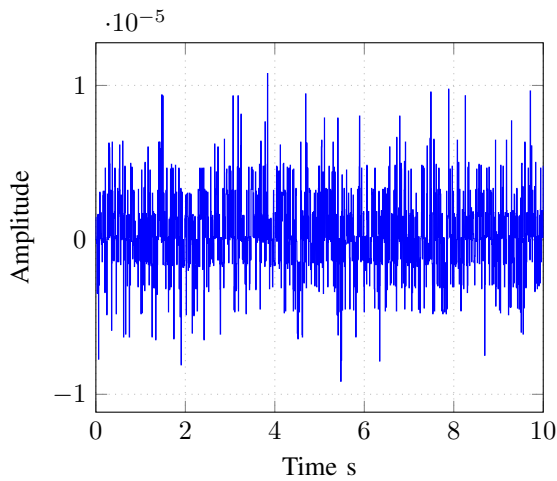


Fig. 22. Sensor measurement noise

A similar approach was taken in capturing process noise. It was assumed that the primary source of process noise would be the current source and the levitator magnet. Therefore, the process noise measurements were taken at a constant input current on the grounding side of the levitator. This ensures that the largest possible process noise is captured.

The noise is then extracted from the current measurement and the process noise covariance is calculated. The process noise covariance was determined to be  $5.22846e - 05$  23.

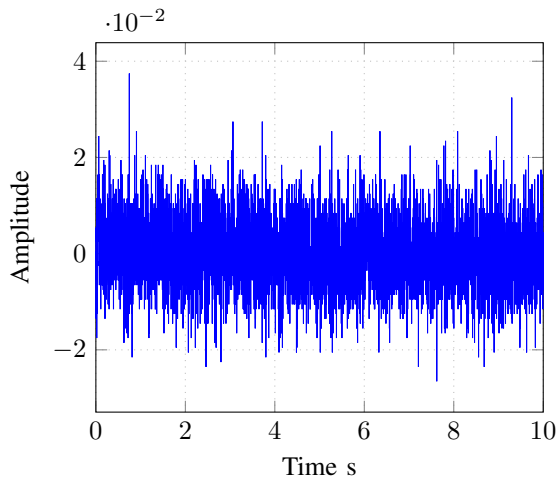


Fig. 23. Current source output noise

1) *PID*: After the model was confirmed to offer an accurate representation of the levitation system, an evaluation of a PID controller was performed. After the stability region calculated was confirmed, proportional, derivative, and integral gain values of 240, 30, and 0.05 were selected as the ‘critically damped’ gain values and were used throughout the PID controller’s evaluation.

The simulated steady-state controller response proved stable with the critically damped PID values selected. With the added Gaussian process and measurement noise the simulated

controller proved stable with an average power draw of 106.6 W. An excess draw of 4.22% of the ideal 102 W steady-state power draw. Applying the same PID gain values to the physical build resulted in an average power draw at steady-state of 110.66 W, showing good agreement with the simulated power consumption with an error of only 3.85% and a total error of 8.23% when compared with the ideal steady-state power consumption 24.

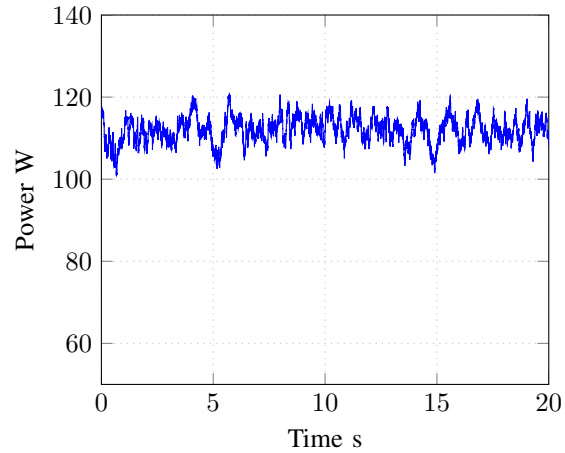


Fig. 24. Steady-state levitator power consumption

With good agreement between the simulated power draw and the power draw seen in the physical build, it is safe to make conclusions on controllers’ topologies by comparing their simulated power draws.

2) *LQR*: Implementation of an optimal gain matrix within the simulated system with the additive process and measurement noise resulted in a steady-state power draw of 102.2452 W. An error of  $2e - 4\%$  compared to the ideal steady-state case. A percentage error improvement of several orders of magnitude when compared with the simulated PID controller.

3) *LQG*: As has been discussed, the Kalman filter built into the LQG controller offers the system a form of noise immunity given an accurate description of the system and the expected process and measurement noise. Given these properties, the average power consumption at steady-state over an extended period of time was 102.245001 W. An error of  $1e - 8\%$  when compared with the ideal steady-state power consumption. As can be seen, the simulated power consumption varies negligibly from the ideal power consumption due to the effects of the Kalman filter embedded within the LQG controller.

4) *Controller Comparisons*: Comparison of the different tested and simulated controller topologies in terms of their average power consumption shows clearly that the optimal controllers offer the best response with negligible excess power draw II. However, it should be noted that the optimal controllers were tested under the assumption that they were developed with perfectly accurate system models. Therefore,

the observers put in place to allow access to all the system's state variables held the same dynamics and measurement characteristics as the physical system. Observers in this case are simulated versions of the physical system that run in parallel with the physical system receiving the same input values and theoretically producing the same state variables. As this system model is not a perfect reflection of the physical system these optimized gains may not be optimal for the physical system. Therefore, it is expected that the real excess power draw of the system while under the regulation of these optimal controllers would be higher than the simulated results.

TABLE II  
POWER CONSUMPTION UNDER REGULATION BY VARIOUS CONTROLLERS

Study Case	Power Consumption [W]
Ideal	102.25
PID Sim	106.56
PID Real	110.66
LQR Sim	102.25
LQG Sim	102.25

## V. CONCLUSIONS AND FUTURE WORKS

The purpose of this project was to develop and evaluate a model for coil-coil interactions in a vertical levitation device. Additionally, several controllers were to be tested/simulated in order to determine which controller topology would provide the most efficient system stabilization in terms of power consumption. The aim was to minimize power consumption in the levitator coil as excess power consumption would reduce the efficiency of the Levitated Dipole Reactor (LDR) employing the use of the two-coil levitation scheme.

Comparing the simulated results for system stability it can be seen that the optimal control methods, LQR and LQG, offer relatively significant reductions in excess power consumption when compared to the PID controller. Compared with the PID controller the LQR controller reduces average power consumption by 4.21% and the LQG controller reduces the power consumption by 4.22% when compared with the simulated PID controller. With the LQG controller offering the least excess power draw of the controller topologies tested, this would be the obvious choice in a system where minimal power draw is required. However, it should be noted that the implementation of either optimal control method is significantly more computationally complex than the PID controller. Therefore, a PID controller may be more suitable depending on the available resources and the level of necessity for an efficient levitation system. Specific applications where excess power dissipation may be required would be in the use of a high-temperature superconducting (HTS) levitator. This is due to HTS operating at low temperatures (60 Kelvin) and therefore any additional heat leak above the minimum required could cause the HTS tape to fail and levitation to cease assuming the cryocooler in use did not have the capabilities to handle the additional heat.

This research is limited largely due to the assumption that an ideal understanding of the system is available in the simulated

models. This assumption offers less realistic results than what would be seen if these controllers were applied to a physical model. Additionally, the modeling of this system's dynamics was constrained to having two coaxial coils. Therefore, a thorough understanding of the system's motion in its other degrees of freedom via simulation is missing.

Future works could include the implementation of the optimal controller topologies within the physical system. Along with an evaluation of their power consumption at steady-state for comparison with the simulated values produced. Additionally, the investigation into the recreation of a 6-dof model, much like the one produced by LDX, and the optimization of several controller topologies for comparisons with the controllers produced for the coaxially constrained model may prove of interest. Finally, the implementation of this model in a Hardware-in-the-loop (HIL) system may prove useful in gaining a better system understanding and in producing a controller optimized for energy efficiency.

## REFERENCES

- [1] Q. Haider, "Nuclear fusion: holy grail of energy," in *Nuclear Fusion-One Noble Goal and a Variety of Scientific and Technological Challenges*, IntechOpen, 2019.
- [2] M. Abdou, E. Vold, C. Gung, M. Youssef, and K. Shin, "Deuterium-tritium fuel self-sufficiency in fusion reactors," *Fusion Technology*, vol. 9, no. 2, pp. 250–285, 1986.
- [3] C. A. Bradley Jr and H. C. Urey, "The relative abundance of hydrogen isotopes in natural hydrogen," *Physical Review*, vol. 40, no. 6, p. 889, 1932.
- [4] R. A. Gross, "Fusion energy," 1984.
- [5] P. Helander, C. Beidler, T. Bird, M. Drevlak, Y. Feng, R. Hatzky, F. Jenko, R. Kleiber, J. Proll, Y. Turkin, *et al.*, "Stellarator and tokamak plasmas: a comparison," *Plasma Physics and Controlled Fusion*, vol. 54, no. 12, p. 124009, 2012.
- [6] J. H. Schultz, J. Kesner, J. Minervini, A. Radovinsky, S. Pourrahimi, B. Smith, P. Thomas, P. Wang, A. Zhukovsky, R. Myatt, *et al.*, "The levitated dipole experiment (ldx) magnet system," *IEEE transactions on applied superconductivity*, vol. 9, no. 2, pp. 378–381, 1999.
- [7] Y. Yano, Z. Yoshida, Y. Ogawa, J. Morikawa, and H. Saitoh, "Feedback control of the position of the levitated superconducting magnet in the rt-1 device," *Fusion engineering and design*, vol. 85, no. 5, pp. 641–648, 2010.
- [8] D. Garnier, A. Hansen, M. Mauel, T. S. Pedersen, J. Bevilacqua, P. Cossa, S. Dagen, J. Kesner, J. Liptac, P. Michael, *et al.*, "Levitation control system for the levitated dipole experiment," in *APS-DPP Meeting, (October, 2001)*, 2001.
- [9] W. Jones, "Earnshaw's theorem and the stability of matter," *European Journal of Physics*, vol. 1, no. 2, p. 85, 1980.
- [10] M. H. Nayfeh and M. K. Brussel, *Electricity and magnetism*. Courier Dover Publications, 2015.
- [11] A. H. Roach, *Floating coil position detection system for the Levitated Dipole Experiment*. PhD thesis, Massachusetts Institute of Technology, 2005.
- [12] C. Chien, *The Hall effect and its applications*. Springer Science & Business Media, 2013.
- [13] W. C. Messner, "Classical control revisited: Variations on a theme," in *2008 10th IEEE International Workshop on Advanced Motion Control*, pp. 15–20, IEEE, 2008.
- [14] M. A. Johnson and M. H. Moradi, *PID control*. Springer, 2005.
- [15] "Bang-bang control." <https://www.techtarget.com/whatis/definition/bang-bang-control>.
- [16] F. L. Lewis, D. Vrabie, and V. L. Syrmos, *Optimal control*. John Wiley & Sons, 2012.
- [17] M. Stoneking, H. Saitoh, M. Singer, E. Stenson, J. Horn-Stanja, T. S. Pedersen, S. Nißl, U. Hergenbahn, N. Yanagi, C. Hugen-schmidt, *et al.*, "Toward a compact levitated superconducting dipole for positron-electron plasma confinement," in *AIP Conference Proceedings*, vol. 1928, p. 020015, AIP Publishing LLC, 2018.

- [18] Y. Yano, Z. Yoshida, J. Morikawa, H. Saitoh, H. Hayashi, and T. Mizushima, "Improvement of field accuracy and plasma performance in the rt-1 device," *Plasma and Fusion Research*, vol. 4, pp. 039–039, 2009.
- [19] L. M. Monzon and J. M. D. Coey, "Magnetic fields in electrochemistry: The lorentz force. a mini-review," *Electrochemistry Communications*, vol. 42, pp. 38–41, 2014.
- [20] M. Mauel, D. Garnier, T. Pedersen, and A. Roach, "Kalman filter for noise reduction and dynamical tracking for levitation control and for plasma mode control," in *APS Division of Plasma Physics Meeting Abstracts*, vol. 46, pp. BP1–113, 2004.
- [21] G. F. Welch, "Kalman filter," *Computer Vision: A Reference Guide*, pp. 1–3, 2020.
- [22] H. I. Nurdin, M. R. James, and I. R. Petersen, "Coherent quantum lqg control," *Automatica*, vol. 45, no. 8, pp. 1837–1846, 2009.
- [23] E. Kriezis, T. D. Tsiboukis, S. M. Panas, and J. A. Tegopoulos, "Eddy currents: Theory and applications," *Proceedings of the IEEE*, vol. 80, no. 10, pp. 1559–1589, 1992.
- [24] J. Lancaster, "Non-ferrous metals," in *Metallurgy of Welding*, pp. 197–223, Springer, 1980.
- [25] "Aluminium specifications." <https://www.steelssupplylp.com/news-and-information/all-about-aluminum#:~:text=Strength%20to%20Weight%20Ratio%20%2D%20An,that%20of%20A36%20carbon%20steel.>
- [26] W. Soud, I. A. Baqer, and M. Ahmed, "Effects on the mechanical properties of the carbon-fiber and polylactic acid specimens," *Engineering and Technology Journal*, vol. 37 part A, pp. 128–132, 04 2019.
- [27] "Tc3 target for matlab and simulink." [https://au.mathworks.com/products/connections/product\\_detail/twincat-3.html.](https://au.mathworks.com/products/connections/product_detail/twincat-3.html)
- [28] "Lv-nh300 sensor." [https://www.keyence.com/products/sensor/laser/lv-n/models/lv-nh300/.](https://www.keyence.com/products/sensor/laser/lv-n/models/lv-nh300/)
- [29] "Sick retroreflective photoelectric sensor." [https://nz.rs-online.com/web/p/photoelectric-sensors/1806362?cm\\_mmc=-PPC-DS3A--\\_google--PLA\\_NZ\\_Pmax\\_Buyer\\_0723-\\_-\\_-&matchtype=&&gad=1&gclid=EAIaIqobChMI2KPEvKfggQMVfGp7Bx3uYgp0EAQYByABEgIOe\\_D\\_BwE&gclid=aw.ds.](https://nz.rs-online.com/web/p/photoelectric-sensors/1806362?cm_mmc=-PPC-DS3A--_google--PLA_NZ_Pmax_Buyer_0723-_-_-&matchtype=&&gad=1&gclid=EAIaIqobChMI2KPEvKfggQMVfGp7Bx3uYgp0EAQYByABEgIOe_D_BwE&gclid=aw.ds)
- [30] "Disoric retroreflective sensor." [https://www.di-soric.com/int-en/PMI/Sensors/Optical-sensors/Optical-distance-sensors?group\\_id=node\\_group\\_g3565\\_en&ix\\_search\[facet\\_finder\\_group\\_t49087\\_prc\\_serie\\_en\]=LAT-45%20Long%20range.](https://www.di-soric.com/int-en/PMI/Sensors/Optical-sensors/Optical-distance-sensors?group_id=node_group_g3565_en&ix_search[facet_finder_group_t49087_prc_serie_en]=LAT-45%20Long%20range)
- [31] "Beckhoff ethercat terminals, el3104." [https://www.beckhoff.com/en-nz/products/i-o/ethercat-terminals/el3xxx-analog-input/el3104.html.](https://www.beckhoff.com/en-nz/products/i-o/ethercat-terminals/el3xxx-analog-input/el3104.html)
- [32] "Beckhoff ethercat terminals, el4034." [https://www.beckhoff.com/en-en/products/i-o/ethercat-terminals/el4xxx-analog-output/el4034.html.](https://www.beckhoff.com/en-en/products/i-o/ethercat-terminals/el4xxx-analog-output/el4034.html)
- [33] "Ldx levitation presentation, darren garnier." OpenStar Technologies, Video Archives.
- [34] J. J. Anagnost and C. A. Desoer, "An elementary proof of the routh-hurwitz stability criterion," *Circuits, systems and signal processing*, vol. 10, no. 1, pp. 101–114, 1991.
- [35] "Be quiet 2, 140mm pwm high speed fan." [https://extremepc.co.nz/be-quiet-pure-wings-2-140mm-pwm-high-speed-case-fan-max-1600-rpm-1/?gclid=CjwKCAjw-KipBhBtEiwAWjgwrA0vaZ\\_0owDhiFCcJIhuxjvTZhnThvaR5u2ZsoKci5z3kMYmBLN0SBoCSXEQA0vD\\_BwE.](https://extremepc.co.nz/be-quiet-pure-wings-2-140mm-pwm-high-speed-case-fan-max-1600-rpm-1/?gclid=CjwKCAjw-KipBhBtEiwAWjgwrA0vaZ_0owDhiFCcJIhuxjvTZhnThvaR5u2ZsoKci5z3kMYmBLN0SBoCSXEQA0vD_BwE)